A theoretical analysis of the electrogastrogram (EGG)

Stefan Calder[1], Leo K. Cheng[1,2] and Peng Du[1]

Abstract— **In this study, a boundary element model was developed to investigate the relationship between the gastric electrical activity, also known as slow waves, and the electrogastrogram (EGG). A dipole was calculated to represent the equivalent net activity of gastric slow waves. The dipole was then placed in an anatomically-realistic torso model to simulate EGG. The torso model was constructed from a laser-scanned geometry of an adult male torso phantom with 190 electrode sites equally distributed around the torso so that simulated EGG could be directly compared between the physical model and the mathematical model. The results were analyzed using the Fast Fourier Transforms (FFT), spatial distribution of EGG potential and a resultant EGG based on a 3-lead configuration. The FFT results showed both the dipole and EGG contained identical dominant frequency component of 3 cycles per minute (cpm), with this result matching known physiological phenomenon. The -3 dB point of the EGG was 110 mm from the region directly above the dipole source. Finally, the results indicated that electrode coupling could theoretically be used in a similar fashion to ECG coupling to gain greater understanding of how EGG correlate to gastric slow waves.**

I. INTRODUCTION

Gastric electrical activity (GEA), also known as slow waves, is a major regulator of gastric motility. Gastric slow waves are autonomously generated and propagated by specialized pacemaker cells called the interstitial cells of Cajal (ICC) and the adjacent smooth muscle cells [5]. Both the pattern and timing of gastric slow wave propagation are fundamental components of digestive function. Gastric slow wave dysrhythmias have been shown to be associated with chronic digestive diseases such as gastroparesis, dyspepsia, and gastroesophageal reflux disease [4].

The accurate in-vivo recording of gastric slow wave is presently limited to relatively invasive recording techniques. Recent high-resolution (HR) mapping studies, using up to 256 electrodes and inter-electrode spacings of 4-7.6 mm, have elucidated that human gastric slows wave originate from a pacemaker region in the proximal corpus along the greater curvature, and exhibit heterogeneous amplitude and speed properties as it propagates towards the pylorus [15][17]. However, due to its invasiveness, HR mapping is limited in its clinical utility. Electrogastrography (EGG) on the other hand, is a non-invasive method of recording the resultant body surface potential of gastric slow wave propagation. The EGG has the ability to give information about slow wave activity in terms of rhythmicity, frequency, amplitude and propagation [3]. EGG therefore holds major potential as a routinely deployable tool to aid the diagnosis of gastric slow wave dysrhythmias and digestive dysfunctions.

The EGG is based on the same fundamental principles as the clinical electrocardiogram (ECG). Since the inception of the ECG in 1887 it has become the most highly used clinical tool for monitoring and diagnosis [8]. However despite the wide spread clinical acceptance of the ECG, the EGG has yet to be adopted by clinicians and is primarily used for research purposes. Hindering the adoption of EGG by clinicians, is the incomplete description of how the cutaneous EGG recordings are characterized in relation to the underlying gastric slow waves [4][1]. Moreover, there is no standardized methodology that has been accepted my the medical and larger research communities, which therefore complicates comparisons made between theoretical and experimental findings [13]. To date the main interpretation method has been limited to correlating the dominant frequency component between EGG and slow waves [4][14]. Another hindrance in its adoption is the low signal to noise ratio (SNR) of the EGG. This is a result of the presence of surrounding organs electrical activity being magnitudes higher than the GEA [16]. The electrical interferences of the surrounding organs cause the GEA to be effectively masked. This presents a signal processing problem of how to isolate the GEA from the other bioelectrical events.

A clear knowledge of the relationship between gastric slow waves and EGG, other than frequency, would be of significant value for determining how the gastric slow wave dysrhythmias develop in chronic digestive diseases [6].

There are many ways one can investigate the correlation of gastric slow waves and EGG both experimentally as well as through multi-scale mathematical modeling. In this study a boundary element model (BEM) was used. BEM has been used in some cases to model EGG, however has been more widely used in both forward and inverse studies of cardiac activity and disease [6][9].

The primary purpose of this study was to identify the relationship between EGG and gastric slow waves, particularly in the spatial domain. In addition we aimed to investigate the spatial distribution of the simulated dipole to identify an effective working area where the simulated EGG signal is above its cut-off frequency. Finally we aimed to investigate the implementation of Einthoven's triangle as a method of interpreting electrode potential voltages.

*This work was supported in part by the New Zealand Health Research Council (HRC), and the US National Institutes of Health (R01 DK64775). Peng Du is supported by a Rutherford Foundation New Zealand Postdoctoral Fellowship and a Marsden Fast-Start Grant.

[1]S. Calder, P. Du and L.K. Cheng are with Auckland Bioengineering Institute, University of Auckland, New Zealand;

[2]L.K. Cheng is also with Department of Surgery, Vanderbilt University, Nashville, TN, USA

978-1-4244-7929-0/14/$26.00 ©2014 IEEE

II. METHODS

The forward model was developed in two steps: (1) a single equivalent dipole was calculated to represent the normal sequence of activation of gastric slow waves; (2) creation of a torso model from a laser scanned geometry of an adult male torso phantom. The simulations were then conducted in the CMISS package (Auckland Bioengineering Institute, New Zealand).

A. Virtual Dipole Source

An equivalent dipole source was calculated from a previously described whole-organ gastric slow wave activation model [6]. Briefly, the biodomain equation was used to solve a system of ordinary differential equations that present slow wave activation of a continuum of gastric tissue containing smooth muscle cells and the ICC. The slow wave activation sequence was solved over a realistic geometry of stomach using the finite element method [6]. A resting membrane potential gradient of -45 to -75 mV was prescribed to the model and the fundus region contained no slow wave activities, in accordance with experimental data [10][19]. Slow wave activation began from a pacemaker region in the greater curvature of the proximal region of the stomach model, and propagated in the aboral direction towards the pylorus region of the stomach, with increasing propagation speed (2.8 mm s^{-1} in the corpus and 5.9 mm s^{-1} in the antrum) and a frequency of 3 cycles-per-minute (cpm). One consequence of the combination of velocity and frequency is the accrual of multiple wavefronts in the stomach, as shown in Fig. 1a. The presence of multiple wavefronts makes a single equivalent dipole with dynamic center less appropriate as it cannot accurately track the activation wavefront and may be located outside the whole geometry. Therefore a static equivalent dipole source was used. The static equivalent dipole source was described by the following equation:

$$\rho = -\frac{\sigma_i \sigma_e}{\sigma_i + \sigma_e} \nabla V_m \tag{1}$$

where V_m represent the simulated membrane potentials, whereas σ_i and σ_e represents the intracellular and extracellular conductivities, respectively.

B. Torso Model

An adult-torso phantom was used to define the anatomy of the torso model. The geometry of the phantom was captured using a three-dimensional (3D) FaroArm scanner (FARO). In addition, 190 evenly spaced ($\sim$50 mm inter-electrode spacing) probe locations were measured to act as specific markers for EGG electrode comparisons. The torso geometry mesh was defined based on the scanned data points ($\sim$2.8 million data points) using an iterative fitting method as previously described [2]. The torso mesh consisted of 254 nodes and 264 elements, the final root mean square error of the fitting procedure was 1.2 mm.

The model was constructed to represent a homogeneous torso and thus did not take into account of any inhomogeneities arising from bone, organs, muscle or subcutaneous fat. These inhomogeneities have been shown in literature to have an effect on the resulting body surface potentials, and will be the subject of future investigations either in vivo or in a more sophisticated phantom setup [12].

The virtual dipole source was placed inside the torso model at a position representing the physiological position of the stomach, as shown in Figure 1d. The BEM was used to solve the Laplace's equation in order to simulate the resultant body-surface potential, i.e., EGG [18].

A mesh convergence analysis was then performed to ensure the accuracy of the output. An iterative convergence scheme was used by halving the element size in each progressive iteration. It was found that after 2 refinements (original number of elements: 264, final number of elements: 1056) the mesh had converged, however a more refined mesh (number of elements: 4024) was used for this study. This convergence can be seen in Figure 1c. The final refined mesh is shown in Figure 1d.

III. RESULTS & DISCUSSION

A. Spectral Analysis

A spectral analysis of the EGG and dipole was performed by applying a fast fourier transform (FFT) in MATLAB (MathWorks, 2013). The result demonstrated that the simulated EGG and dipole contained identical dominant frequency of 3 cycles per minute (cpm), as shown in Figure 2. This result agreed with previous experimental studies of EGG [4][14]. Interferences from other physiological sources, e.g., cardiac electrical activity, were not investigated in this study. This limitation will need to be addressed since cardiac electrical activity is a magnitude higher in amplitude than gastric slow waves. Nevertheless, the spectral analysis confirmed the direct correlation of frequency between EGG and gastric slow waves.

Figure 2 also shows large variance in amplitude between the input and output. This variance could be attributed to attenuation of the signal due to distance traveled by the signal and will be discussed further in the subsequent section of this paper.

B. Spatial Analysis

The amplitude of the simulated EGG relative to the location of the highest potential on the torso was quantified, as shown in Figure 3. A line of best fit was then fitted to the data and a residual plot drawn, seen in Figure 3.

The relative amplitude of EGG increased with distance away from the location of the highest potential, which was located on the torso model directly above the dipole. This result is an expected result as it is commonly known that current will follow the path of least resistance. Since the resistance is dependent on the distance that the current must travel through the torso, it follows that the further the probe is away from the source terminal the smaller the current and change in potential. Based on this trend the half power point was calculated to establish an effective working radius. The cut-off distance was found to be $\sim$110 mm from the voltage source.

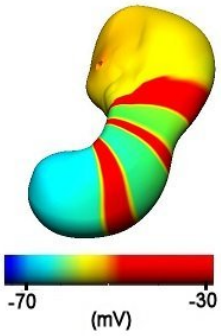

(a) Visualization of gastric slow waves

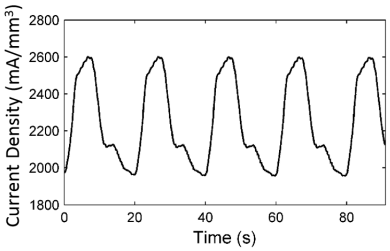

(b) Signal representation of gastric slow waves

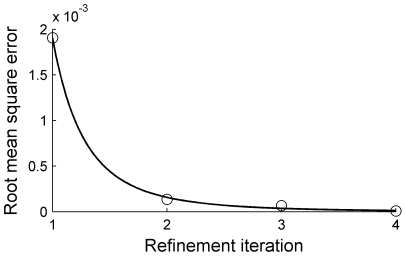

(c) Mesh Refinement

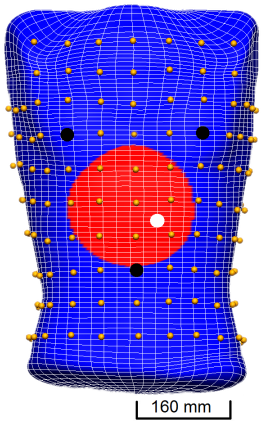

(d) Fitted Torso Model

Fig. 1. Setup of forward simulation of electrogastrogram (EGG). a) Visualization of input signal in stomach model previously described [7]. b) This figure shows a trace of the input signal representing the stomach gastric slow wave over a 90s time period c) Results from the mesh refinement. After 2 refinements it was determined that any further refinements would have negligible effects on results. d) This figure shows the final fitted torso model with a total of 4224 elements. The red area indicates the effective working radius (at a specific instance in time) whilst the blue shows the area outside the half power point. In addition spheres represent probe locations and dipole locations (Gold: regular EGG electrodes, Black: Einthoven's triangle electrodes, White: equivalent dipole source).

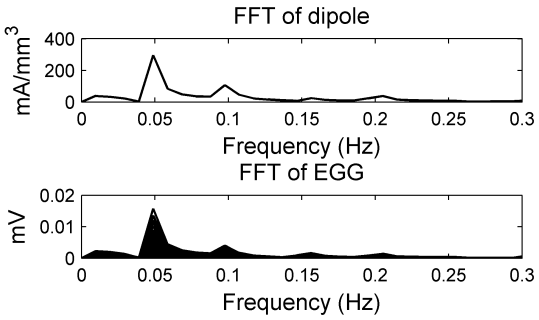

Fig. 2. A spectral analysis of the input signal and the output signal from all 190 probe locations. The dominant frequency in the dipole and EGG was identical.

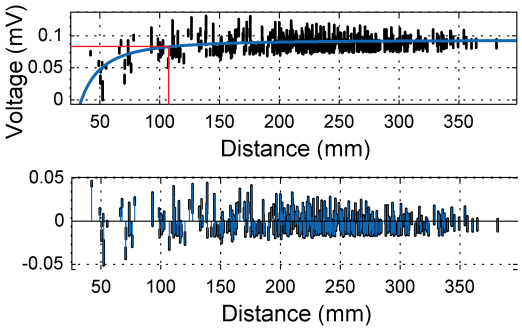

Fig. 3. Relation between distance and voltage potential. A power series trend line was fitted to the data. At approximately 110 mm the half power point can be seen, the trend line shows the same effect with the voltage potential nearly plateauing and thus indicating any point beyond 110 mm had near negligible voltage. The lower plot is a residual plot which also shows as distance increases variance decreases.

The variance of the potential differences decreased as the distance increased, as shown in Figure 3. This particular trend was attributed to the directionality of the dipole, i.e., the EGG potential simulated at electrodes that were in the direction of the dipole vector had higher potentials than those that were not the direction of the dipole vector. Those probes that were in the path or direction of the simulated vector had much higher voltages than those next to them.

This relationship between distance, voltage potential and directionality may infer that future studies should have a more dense localization of probe points within 110 mm of the dipole source rather than equally distributed around the entire domain as was done in this study.

C. EGG lead analysis

Based on the results from the spatial analysis a 5x5 electrode array was identified to cover the 110 mm sensitive EGG distance. Three EGG leads were constructed from the electrode array to form a basic Einthoven's triangle, as shown Figure 4a. The potential differences between these three leads were calculated, output from these calculations can be seen in Figure 4b. This figure shows that Lead I closely resembles the input data, Lead III resembles input signal with a phase delay of 180 degrees, whilst comparatively Lead II's data appears to have little familiarity with the input signal.

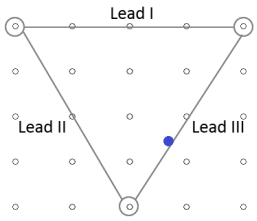

(a) EGG Einthoven's triangle

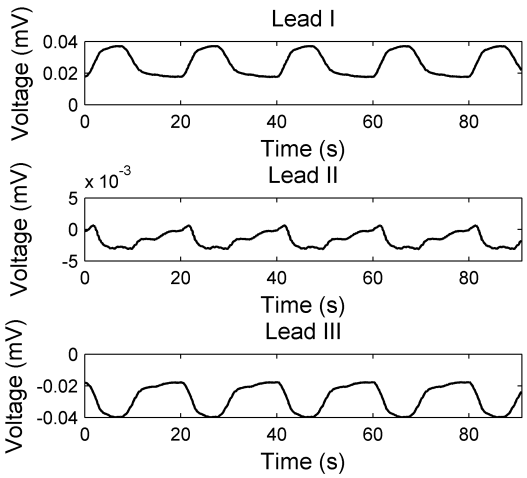

(b) EGG lead analysis

Fig. 4. a) Shows a 5x5 grid with the equivalent dipole (shown in blue) representing a 200x200 mm area within the distance tolerance. Based on ECG recording techniques 3 locations have been chosen to act as EGG equivalents. b) Simulated lead output based on the gastric slow waves. We see that Lead I closely follows the input signal, whilst Lead III seems to be the inverse. Comparatively Lead II's waveform shape has little familiarity with the original input source.

Of the three leads analyzed Lead I shows the most promise for use as a EGG lead. Although this lead does not have the exact same trend as the dipole signal, it does suggest that with further refinement and further research a more direct correlation between the EGG and gastric slow waves will be further established.

IV. CONCLUSIONS & FUTURE WORK

A forward model of EGG in an anatomically-realistic torso model was developed. The analysis focused on the spatial correlation between EGG and gastric slow waves represented by an equivalent dipole.

A direct correlation between the voltage potential and the distance away from the source was found. The results showed that after approximately 110 mm the EGG signal amplitude become negligible, and thus in future studies it may be of further benefit to have a higher electrode density within this area [11]. A critical next step is to validate the model by experimentally reproducing the dipole in a torso tank setup, and then comparing the recorded torso potential to the simulated EGG. In subsequent work we intend to include alternative sources (e.g. heart source) to closer represent realistic conditions. Furthermore a key next step is to quantitatively identify the correlation between EGG and gastric slow waves in both in-vitro and in-vivo conditions.

REFERENCES

[1] M Bortolotti, *Electrogastrography: a seductive promise, only partially kept.*, The American journal of gastroenterology **93** (1998), no. 10, 1791–4.

[2] M L Buist, L K Cheng, K M Sanders, and A J Pullan, *Multiscale modelling of human gastric electric activity: can the electrogastrogram detect functional electrical uncoupling?*, Experimental physiology **91** (2006), no. 2, 383–90.

[3] F Y Chang, *Electrogastrography: basic knowledge, recording, processing and its clinical applications.*, Journal of gastroenterology and hepatology **20** (2005), no. 4, 502–16.

[4] J D Chen, B D Schirmer, and R W McCallum, *Serosal and cutaneous recordings of gastric myoelectrical activity in patients with gastroparesis.*, The American journal of physiology **266** (1994), no. 1 Pt 1, G90–8.

[5] L K Cheng, G O'Grady, P Du, J U Egbuji, J A Windsor, and A J Pullan, *Gastrointestinal system.*, Wiley interdisciplinary reviews. Systems biology and medicine **2** (2010), no. 1, 65–79.

[6] P Du, G O'Grady, L K Cheng, and A J Pullan, *A multiscale model of the electrophysiological basis of the human electrogastrogram.*, Biophysical journal **99** (2010), no. 9, 2784–92.

[7] P Du, G O'Grady, J Gao, S Sathar, and L K Cheng, *Toward the virtual stomach: progress in multiscale modeling of gastric electrophysiology and motility.*, Wiley interdisciplinary reviews. Systems biology and medicine **5** (2013), no. 4, 481–93.

[8] D B. Geselowitz, *On the theory of the electrocardiogram*, Proceedings of the IEEE **77** (1989), no. 6, 857–876.

[9] R.M. Gulrajani, *The forward and inverse problems of electrocardiography*, Engineering in Medicine and Biology Magazine, IEEE **17** (1998), no. 5, 84–101, 122.

[10] G D S Hirst and F R Edwards, *Electrical events underlying organized myogenic contractions of the guinea pig stomach.*, The Journal of physiology **576** (2006), no. Pt 3, 659–65.

[11] J H K Kim, P Du, and L K Cheng, *Reconstruction of normal and abnormal gastric electrical sources using a potential based inverse method.*, Physiological measurement **34** (2013), no. 9, 1193–206.

[12] R N Klepfer, C R Johnson, and R S Macleod, *The effects of inhomogeneities and anisotropies on electrocardiographic fields: a 3-D finite-element study.*, IEEE transactions on bio-medical engineering **44** (1997), no. 8, 706–19.

[13] J Levy, J Harris, J Chen, D Sapoznikov, B Riley, W De La Nuez, and A Khaskelberg, *Electrogastrographic norms in children: toward the development of standard methods, reproducible results, and reliable normative data.*, Journal of pediatric gastroenterology and nutrition **33** (2001), no. 4, 455–61.

[14] Z Lin, J D Chen, B D Schirmer, and R W McCallum, *Postprandial response of gastric slow waves: correlation of serosal recordings with the electrogastrogram.*, Digestive diseases and sciences **45** (2000), no. 4, 645–51.

[15] G O'Grady, T R Angeli, P Du, C Lahr, W J E P Lammers, J A Windsor, T L Abell, G Farrugia, A J Pullan, and L K Cheng, *Abnormal initiation and conduction of slow-wave activity in gastroparesis, defined by high-resolution electrical mapping.*, Gastroenterology **143** (2012), no. 3, 589–98.e1–3.

[16] G O'Grady, P Du, J U Egbuji, W J E P Lammers, A Wahab, A J Pullan, L K Cheng, and J A Windsor, *A novel laparoscopic device for measuring gastrointestinal slow-wave activity.*, Surgical endoscopy **23** (2009), no. 12, 2842–8.

[17] G O'Grady, A J Pullan, and L K Cheng, *The analysis of human gastric pacemaker activity.*, The Journal of physiology **590** (2012), no. Pt 5, 1299–300; author reply 1301–2.

[18] A J Pullan, M L Buist, G B Sands, L K Cheng, and N P Smith, *Cardiac electrical activity–from heart to body surface and back again.*, Journal of electrocardiology **36 Suppl** (2003), 63–7.

[19] K M Sanders, S D Koh, and S M Ward, *Interstitial cells of cajal as pacemakers in the gastrointestinal tract.*, Annual review of physiology **68** (2006), 307–43.